Q. J. R. Meteorol. Soc. **00**: 1–12 (2008)
Published online in Wiley InterScience
(www.interscience.wiley.com) DOI: 10.1002/qj.000

A mass-conservative version of the semi-implicit semi-Lagrangian HIRLAM

P. H. Lauritzen[a], E. Kaas[b], B. Machenhauer[c] and K. Lindberg[c]
[a]*National Center for Atmospheric Research*[†]*, Boulder, USA*
[b]*University of Copenhagen, Copenhagen, Denmark*
[c]*Danish Meteorological Institute, Copenhagen, Denmark*

Abstract: A mass-conservative version of the semi-implicit semi-Lagrangian High-Resolution Limited Area Model (HIRLAM) is presented. The explicit continuity equation is solved with the so-called cell-integrated semi-Lagrangian (CISL) method. To allow for long time steps the CISL scheme is coupled with a recently developed semi-implicit time-stepping scheme that involves the same non-complicated elliptic equation as in HIRLAM. Contrarily to the traditional semi-Lagrangian method the trajectories are backward in the horizontal and forward in the vertical, that is, cells moving with the flow depart from model layers and arrive in a regular column, and their vertical displacements are computed from continuity of mass and hydrostatic balance in the arrival column. This involves just two-dimensional upstream integrals and allows for a Lagrangian discretization of the energy conversion term in the thermodynamic equation.
Preliminary validation of the new model version is performed using an idealized baroclinic wave test case. The accuracy of the new formulation of HIRLAM is comparable to the reference version though it is slightly more diffusive. A main finding is that the new discretization of the energy conversion term leads to more accurate simulations compared to the traditional 'Eulerian' treatment.

KEY WORDS Advection; Baroclinic model; Cascade Interpolation; Conservation; Finite Volume; Semi-Lagrangian

Received 28 December 2007; Revised 22 May 2008; Accepted 17 July 2008

1 Introduction

The semi-Lagrangian method for advection together with a semi-implicit treatment of the gravity wave terms is well known to be an efficient and accurate numerical method for atmospheric models (for a review see Staniforth and Côté 1991). A deficiency of the semi-Lagrangian semi-implicit method is the lack of formal mass-conservation. The mass-conservation can be restored by the application of so-called mass-fixers that repeatedly restore global mass-conservation. However, mass-fixers are not completely satisfactory since the mass restoration is not local, so mass is not added where spurious sinks have removed mass (and vice versa). A first step toward a locally mass-conservative semi-Lagrangian semi-implicit model has been taken with the development of the cell-integrated semi-Lagrangian (CISL), or equivalently, finite-volume semi-Lagrangian advection scheme (e.g., Nair and Machenhauer 2002). For a recent review of finite-volume methods used in meteorology see Machenhauer *et al.* (2007) and the detailed stability analysis given in Lauritzen (2007).

A semi-implicit time-stepping of the fast waves requires that the term involving the flow divergence in the continuity equation must be handled in a semi-implicit manner. As described in Machenhauer and Olk (1997), when the mass equation is discretized using a CISL scheme the flow divergence appears only in the way the trajectories determine Lagrangian departure volumes, and therefore the Lagrangian divergence should be computed implicitly. This, however, leads to a complicated elliptic system as shown in detail in Lauritzen (2005) and Thuburn (2007). To retain a simpler elliptic system as in HIRLAM we chose a 'predictor-corrector' approach (Lauritzen *et al.* 2006, hereinafter referred to as LKM06).

The semi-Lagrangian component of the model obviously involves the determination of the characteristics. Here we track cells moving with the flow that depart from a model layer and arrive in a vertical column of regular Eulerian grid cells in the horizontal (Machenhauer and Olk 1998) but at vertical levels that are different from the model levels. That is, a cell originating from a particular model layer moves forward and with vertical walls along the backward trajectories determined from horizontal winds (Fig. 1). So in the horizontal the trajectories are backward and in the vertical they are forward. Consequently, the upstream integral, which determine the mass advected into the regular column is two-dimensional, and existing two-dimensional CISL methods are directly applicable. Contrarily to conventional fully three-dimensional upstream trajectory algorithms where the vertical displacements are computed from time-extrapolated vertical displacements, we use the CISL continuity equation to determine the mass-flux into

*Correspondence to: NCAR, 1850 Table Mesa Drive, Boulder, CO 80307-3000, USA. E-mail: pel@ucar.edu
[†]The National Center for Atmospheric Research is sponsored by the National Science Foundation

the arrival column and can then determine the vertical displacements from hydrostatic balance. Hereby the pressure at the top of a mass cell transported into the arrival column is obtained as a diagnostic variable. This is used for a simple Lagrangian discretization of the vertical velocity in pressure coordinates given by the difference between the pressure over the departure cell and the hydrostatically determined pressure over the arrival cell divided by the time step. Since the parcel trajectories are forward in the vertical, they generally do not arrive at model layers, and therefore a vertical remapping of the prognostic variables back to model layers must be performed (Machenhauer and Olk 1998; Lin 2004). These remappings are, however, only one-dimensional. This concept of 'floating Lagrangian surface', along which the Lagrangian cells here in fact are moving during a time step, was theoretically introduced by Starr (1946). With this reference the concept has been utilized also by Lin (2004) and Nair and Tufo (2007).

The paper is organized as follows. In Section 2 the continuous primitive equations are reformulated for the new model. In Section 3 the discretization of the equations is presented which encompasses the Eulerian discretization grid, discretization of the hydrostatic equation, new trajectory algorithm, explicit CISL continuity equation and the semi-implicit CISL continuity equation. The remaining equations of motion are discretized using a grid point representation as in HIRLAM, but modified for the hybrid trajectory and the Lagrangian discretization of the energy conversion term in the thermodynamic equation. Finally, the CISL continuity equation for tracers and the vertical remapping are discussed. Section 4 contains preliminary results from tests of the new dynamical core followed by conclusions and a discussion in Section 5.

2 Reformulation of the primitive equations

Consider the equations for a quasi-hydrostatic and moist-diabatic atmosphere using the vertical coordinate, $\eta(p, p_s)$, introduced by Simmons and Burridge (1981):

$$\frac{du}{dt} = -\frac{1}{a\cos\theta}\frac{\partial\Phi}{\partial\lambda} - \frac{R_d T_v}{p}\frac{1}{a\cos\theta}\frac{\partial p}{\partial\lambda} + f v + \frac{uv}{a}\tan\theta + P_u + K_u, \quad (1)$$

$$\frac{dv}{dt} = -\frac{1}{a}\frac{\partial\Phi}{\partial\theta} - \frac{R_d T_v}{p}\frac{1}{a}\frac{\partial p}{\partial\theta} - f u - \frac{u^2}{a}\tan\theta + P_v + K_v, \quad (2)$$

$$\frac{dT}{dt} = \frac{R_d T_v}{c_p}\frac{\omega}{p} + P_T + K_T, \quad (3)$$

$$\frac{d}{dt}\left(\ln\frac{\partial p}{\partial\eta}\right) = -D - \frac{\partial\dot{\eta}}{\partial\eta}, \quad (4)$$

$$\frac{\partial\Phi}{\partial\eta} = -\frac{R_d T_v}{p}\frac{\partial p}{\partial\eta}, \quad (5)$$

where t is time, λ is the longitude, θ the latitude, a the radius of the earth, f the Coriolis parameter, u and v are the horizontal wind components towards east and north, respectively, Φ the geopotential, p the pressure, $\omega = dp/dt$ the vertical velocity in pressure coordinates, T the temperature, D the divergence, and T_v the virtual temperature given by

$$T_v = T\left[1 + \left(\tfrac{1}{\epsilon} - 1\right) q\right], \quad (6)$$

$$\epsilon = \frac{R_d}{R_v}, \quad (7)$$

and the total derivative and specific heat capacity are given by

$$\frac{d}{dt} \equiv \frac{\partial}{\partial t} + \frac{u}{a\cos\theta}\frac{\partial}{\partial\lambda} + \frac{v}{a}\frac{\partial}{\partial\theta} + \dot{\eta}\frac{\partial}{\partial\eta}, \quad (8)$$

$$c_p = c_{pd}\left[1 + \left(\tfrac{c_{pv}}{c_{pd}} - 1\right) q\right], \quad (9)$$

respectively, and $\dot{\eta}$ is the η-coordinate vertical velocity. R_d and R_v are the gas constants for dry air and water vapor, respectively, and c_{pd} and c_{pv} are the specific heat capacity of dry air and water vapor at constant pressure. Finally, the terms K_T, K_u, and K_v represent horizontal diffusion processes, and P_T, P_u, and P_v represent physical processes.

The continuity equation (5) is reformulated to use the CISL approach by expanding the left-hand side and replacing the right-hand side, which is the three-dimensional divergence, with its Lagrangian form

$$\frac{1}{\delta V}\frac{d\,\delta V}{dt}, \quad (10)$$

where δV is an infinitesimal volume element in the (λ, θ, η)-coordinate system. Making use of the chain rule for differentiation, the Lagrangian form of the continuity equation can be written as

$$\frac{d}{dt}\left(\frac{\partial p}{\partial\eta}\,\delta V\right) = 0, \quad (11)$$

(e.g., Machenhauer 1994). Equations (1), (2), (4), (6) and (11) form the basis for the discretizations in the new model version.

3 Discretization of the primitive equations

3.1 Discretization grid

In the horizontal the Arakawa C-grid defines the Eulerian grid cells and grid points. The prognostic mass variable is the mass integrated over a regular Eulerian grid cell with velocity component grid points at its sides (Fig. 3 in LKM06). The points in the centre of the Eulerian mass cells are called mass points. They are also temperature grid points.

Following Simmons and Burridge (1981), the atmosphere is divided into $NLEV$ layers and the layer index is increasing toward the surface. The pressure at the interface between layer k and $k+1$ is defined by the pressure

$$p^{eul}_{k+1/2} = A_{k+1/2} + B_{k+1/2}\, p_s, \quad (12)$$

DOI: 10.1002/qj

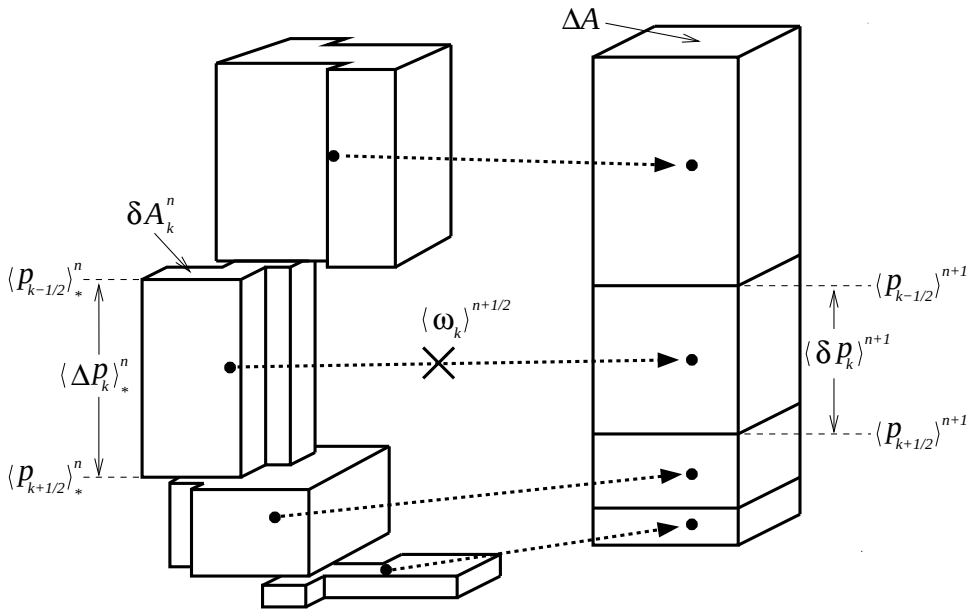

Figure 1. Schematic illustration of the departure and arrival cells, which make up the deformed column on the left and the regular column on the right, respectively (in the special case where all cells in each model level have the same pressure thickness). The cells move with vertical walls and the horizontal extension is a polygon. In this Figure the polygon is as in the two-dimensional CISL scheme of Nair and Machenhauer (2002), but the general idea applies to all CISL schemes. $\langle \Delta p_k \rangle_*^n$ is the integral mean value of the pressure-layer thickness over the irregular departure cell area δA_k^n, and $\langle \delta p_k \rangle^{n+1}$ is the mean value of the pressure-layer thickness over the regular arrival cell area ΔA. The average pressure at the bottom of the arrival cell is denoted $\langle p_{k+1/2} \rangle^{n+1}$ and is given by the weight of the air above it (see (29)). Knowing the average pressure over the departure and arrival cell, $\langle p_k \rangle_*^n$ and $\langle p_k \rangle^{n+1}$ respectively, the vertical velocity $\langle \omega_k \rangle^{n+1/2}$ may simply be discretized in a Lagrangian fashion in terms of the difference between these average pressures (see (33)). Since the trajectories are forward in the vertical the vertical location of the arrival cells $\langle p_{k+1/2} \rangle^{n+1}$ is different from the new Eulerian hybrid model level $\langle p_{k+1/2}^{eul} \rangle^{n+1}$ determined by the new surface pressure and hybrid coefficients (13).

where $A_{k+1/2}$ and $B_{k+1/2}$ are predefined constants, p_s is the surface pressure and $0 \leq k \leq NLEV$. The vertical index $k+1/2$ refers to a 'half level' and the pressure $p_{k+1/2}$ is the pressure at the 'bottom' of the cell with vertical index k. In HIRLAM the pressure at the top of the atmosphere $p_{1/2}$ is set to zero. The pressure thickness of layer k is denoted $\Delta p_k = p_{k+1/2} - p_{k-1/2}$. In between the half levels are the 'full levels' and their exact location is discussed in the next Section. The vertical staggering of the dependent variables is a Lorenz-type staggering in which T, u and v are at the full levels and the geopotential, pressure, and vertical velocity are at half levels.

3.2 Hydrostatic equation

Since the pressure gradient force involves the horizontal gradient of Φ_k in the momentum equations, the full level geopotential Φ_k is needed. Hence the discretization of the pressure gradient force is related to the hydrostatic equation. The finite-difference analogue of the hydrostatic equation (6) for a single layer and for the air mass from the surface and up to half level $k+1/2$ is given by

$$\Phi_{k+1/2} - \Phi_{k-1/2} = -R_d \, (T_v)_k \, (\Delta \ln p)_k \,, \tag{14}$$

$$\Phi_{k+1/2} = \Phi_s + R_d \sum_{\ell=k+1}^{NLEV} (T_v)_\ell \, (\Delta \ln p)_\ell \,, \tag{15}$$

respectively, where

$$(\Delta \ln p)_k \equiv \ln \left(\frac{p_{k+1/2}}{p_{k-1/2}} \right). \tag{16}$$

To get Φ_k the popular approach by Simmons and Burridge (1981) is used

$$\Phi_k = \Phi_{k+1/2} + \alpha_k \, R_d \, (T_v)_k, \tag{17}$$

where the last term on the right-hand side of (17) is an approximation to

$$R_d \int_{p=p_k}^{p=p_{k+1/2}} T_v \, d \ln p. \tag{18}$$

Under the assumption that T_v is constant equal to $(T_v)_k$ over the half layer, $p = p_k$ to $p = p_{k+1/2}$, α_k is the approximation to the integral

$$\int_{p=p_k}^{p=p_{k+1/2}} d \ln p. \tag{19}$$

Simmons and Burridge (1981) approximates α_k with

$$\alpha_k = \begin{cases} \ln 2 & , \text{ for } k = 1, \\ 1 - \frac{p_{k-1/2}}{\Delta p_k} \, (\Delta \ln p)_k & , \text{ for } k = 2, .., NLEV. \end{cases} \tag{20}$$

This approximation is used here as well.

DOI: 10.1002/qj

For the discretizations in the trajectory algorithm the pressure (which is held at half levels) is needed at full levels in the new HIRLAM version. Equation (19) is used to define the full level pressure consistent with the definition of α_k:

$$p_k = p_{k+1/2}\, \exp\left(-\alpha_k\right), \tag{21}$$

where the integral constant has been set to zero so that $p_1 = \frac{1}{2}p_{3/2}$. Equation (21) is slightly different from the approximation $p_k = (p_{k+1/2} + p_{k-1/2})/2$ used in the current operational HIRLAM.

3.3 The explicit CISL equations

As indicated in the introduction and illustrated in Figure 1 the mass transport is modeled by finite volumes that originate at time $t = n\,\Delta t$ from a model layer k, move with vertical walls with the three dimensional flow and end up at time $t = (n+1)\,\Delta t$ in a regular grid column (arrival column). We will call such a moving finite volume a *Lagrangian cell*. The mass in a Lagrangian cell with thickness $\delta z = z_2 - z_1$ is at a certain time:

$$\begin{aligned} M_{\delta V} &= \iint_{\delta A}\left(\int_{z_1}^{z_2}\rho\, dz\right) dA = \frac{1}{g}\iint_{\delta A}\delta p\, dA \\ &= \frac{1}{g}\langle\delta p\rangle\delta A, \end{aligned} \tag{22}$$

where the hydrostatic equation $dp = -g\rho\, dz$ was used in the inner integral. Thus, the condition for local mass-conservation is

$$\frac{d\left(M_{\delta V}\right)}{dt} = \frac{1}{g}\frac{d}{dt}\left(\langle\delta p\rangle\delta A\right) = 0. \tag{23}$$

Here, *local mass-conservation* is defined as conservation of the mass of individual Lagrangian cells. From (23) the CISL continuity equation for moist air is obtained by integration in time from $n\Delta t$ to $(n+1)\Delta t$. It may be written as

$$\langle\delta p_k\rangle_{\text{expl}}^{n+1} = \langle\Delta p_k\rangle_*^n \frac{\delta A_k^n}{\Delta A}, \tag{24}$$

where

$$\langle\Delta p_k\rangle_*^n = \frac{1}{\delta A_k^n}\iint_{\delta A_k^n} S(\langle\Delta p_k\rangle)\, dA. \tag{25}$$

A sub-script 'expl' has been added in (24) to distinguish the updated value from that in the semi-implicit continuity equation (47) to be presented in Section 3.4.2. Note, that brackets $\langle\cdot\rangle$ denote a mean value over a regular grid area ΔA whereas a mean value over an irregular departure area δA_k^n, as defined in (25), is denoted $\langle\cdot\rangle_*^n$ (Figure 1). $S(\langle\Delta p_k\rangle)$ refers to the sub-grid-scale representation based on the known Eularian cell averaged values $\langle\Delta p_k\rangle$ at time level n. Depending on the CISL advection scheme the departure area δA_k^n at a certain model level k is determined by straight-line segments connecting the departure points of four trajectories. Each of these is ending up in a corner point of the arrival area ΔA at the pressure level p_k^{n+1}. Note that p_k^{n+1} is the cell averaged pressure at full level $\langle p_k\rangle^{n+1}$ interpolated to the corner point in question.

In traditional semi-Lagrangian models as HIRLAM all three dimensions of the departure point position are determined iteratively from given time-extrapolated three-dimensional velocity vectors (e.g., Ritchie 1991). In the iterative procedure of the present mass-conservative HIRLAM version, given horizontal wind vectors determine just the horizontal position of the departure point whereas the vertical position of the arrival point, that is the updated Lagrangian pressure $\langle p_k\rangle_{\text{expl}}^{n+1}$, is calculated from hydrostatic balance in the arrival cell columns; after the quasi-horizontal displacements of mass cells determined by the CISL continuity equation have taken place. As a by-product the difference between the arrival pressure and the departure pressure of Lagrangian cells divided by the time step determines a mean vertical velocity along the trajectories. This Lagrangian vertical velocity is used in the energy conversion term of the thermodynamic equation instead of the Eulerian vertical velocities used in traditional semi-Lagrangian models as HIRLAM.

For a certain trajectory in level k let the ith iteration of the horizontal position vector of the departure point and the position vector of the arrival point be called $\mathbf{r}_*$ and $\mathbf{r}$, respectively. Then $\mathbf{r}_*$ is determined by

$$\mathbf{r}_* = \mathbf{r} - \langle\mathbf{V}\rangle\Delta t. \tag{26}$$

Here $\langle\mathbf{V}\rangle$ is an averaged horizontal wind vector along the trajectory. It is approximated by

$$\langle\mathbf{V}\rangle = \frac{1}{2}\mathbf{V}_*^n + \frac{\Delta t}{8}\frac{d\mathbf{V}_*^n}{dt} + \frac{1}{2}\widetilde{\mathbf{V}}^{n+1} - \frac{\Delta t}{8}\frac{d\widetilde{\mathbf{V}}^{n+1}}{dt}, \tag{27}$$

where $(\,)_*^n$ and $(\,)^{n+1}$ denote values interpolated to the departure point $(\mathbf{r}_*, p_*^n)$ and the arrival point $\left(\mathbf{r}, p_{\text{expl}}^{n+1}\right)$, respectively, for which cubic Lagrange interpolation is used. $\widetilde{\mathbf{V}}^{n+1} = 2\mathbf{V}^n - \mathbf{V}^{n-1}$ is the time-extrapolated horizontal wind valid at time $t = (n+1)\Delta t$. The accelerations in (27) are approximated with

$$\frac{d\mathbf{V}}{dt} \approx \mathbf{V}\cdot\nabla\mathbf{V}. \tag{28}$$

(McGregor 1993). The initial condition for the iteration is $\mathbf{r}_* = \mathbf{r}$ and $p_*^n = (p_k^{\text{eul}})^n$. The wind components are interpolated from their C-grid positions to the grid cell vertices, where they are needed in (27), using cubic Lagrangian interpolation.

When in a certain iteration the four corner points $\mathbf{r}_*$ of the departure cell at model layer k have been determined from (26) the horizontal upstream area δA_k^n can be constructed and the mass transport from this model layer into the arrival column can be computed using the explicit CISL continuity equation (24). The two-dimensional integral in (25) is computed by a CISL scheme. Here we use the scheme of Nair and Machenhauer (2002) or alternately the cascade scheme of Nair *et al.* (2002) both using a parabolic sub-grid-scale representation. When the mass transported into the arrival column from all NLEV

DOI: 10.1002/qj

model layers (Figure 1) have been computed, the cell averaged pressure at the bottom of each Lagrangian cell $\langle p_{k+1/2}\rangle^{n+1}_{\text{expl}}$ can be determined by the assumption of hydrostatic balance. This implies simply that it is the weight of the air mass above the cell bottom:

$$\langle p_{k+1/2}\rangle^{n+1}_{\text{expl}} = \sum_{l=1}^{k} \langle p_l\rangle^{n+1}_{\text{expl}}. \tag{29}$$

The cell averaged pressure at full levels is obtained from (21):

$$\langle p_k\rangle^{n+1}_{\text{expl}} = \exp\left\{-\langle \alpha_k\rangle^{n+1}_{\text{expl}}\right\} \langle p_{k+1/2}\rangle^{n+1}_{\text{expl}}, \tag{30}$$

where $\langle \alpha_k\rangle^{n+1}_{\text{expl}}$ results by substituting $\langle p_{k+1/2}\rangle^{n+1}_{\text{expl}}$, determined from (29), for $p_{k-1/2}$ in the formula for α_k (20). The procedure is then iterated.

It was found empirically that two iterations of the trajectory algorithm are sufficient. Using the values determined from the final iteration also the explicit updated cell averaged surface pressure $\langle p_s\rangle^{n+1}_{\text{expl}}$ can be determined from the assumption of hydrostatic balance:

$$\langle p_s\rangle^{n+1}_{\text{expl}} = \sum_{k=1}^{NLEV} \langle \delta p_k\rangle^{n+1}_{\text{expl}}. \tag{31}$$

Using these surface pressures in (13) explicit updated Eulerian half levels may be determined.

For a global model version global mass-conservation follows from (31). This is seen by substituting (24) in (31), multiplying the result by Δt and sum over all horizontal grid cells

$$\sum_{i=1}^{I}\sum_{j=1}^{J}\sum_{k=1}^{NLEV} \langle \delta p_{ijk}\rangle^{n+1}_{\text{expl}} \Delta A_{ij} = \sum_{i=1}^{I}\sum_{j=1}^{J}\sum_{k=1}^{NLEV} \langle \Delta p_{ijk}\rangle^{n}_{*} \delta A^n_{ijk}, \tag{32}$$

where I and J is the number of Eulerian grid cells in the zonal and meridional direction, respectively. At each level k the departure areas are constructed such that the sum of all departure areas $\sum_{i=1}^{I}\sum_{j=1}^{J}\delta A^n_{ijk}$, like the sum of Eulerian grid areas $\sum_{i=1}^{I}\sum_{j=1}^{J}\Delta A_{ij}$, is equal to the global area. The right-hand side of (32) is the weight of the total mass at time t, which according to (32) is equal to the weight of the total mass at time $t+\Delta t$. Thus the total mass is conserved.

In the case of a limited area model, as the present HIRLAM version, the left-hand side is still the weight of the total mass in the total limited integration area at time $t+\Delta t$, which according to (32) is equal to the weight of the total mass in the total upstream departure area $\sum_{i=1}^{I}\sum_{j=1}^{J}\delta A^n_{ijk}$ at time t. However, these areas vary generally from time step to time step and differ from level to level, so consequently, the total mass in the integration area will change during each time step. The change is equal to the difference between the total inflow and the total outflow through the limited area boundary. Generally, further changes in the total mass in the integration area will result from the boundary relaxation performed at the end of the time step.

As already mentioned, we discretize the vertical velocity $\omega = dp/dt$ on the right-hand side of the explicit thermodynamic equation (4) in a Lagrangian fashion, that is, the mean value $\langle \omega_k\rangle^{n+1/2}_{\text{expl}}$ of ω along the trajectories for a cell departing from level k is determined by

$$\langle \omega_k\rangle^{n+1/2}_{\text{expl}} = \frac{1}{\Delta t}\left[\langle p_k\rangle^{n+1}_{\text{expl}} - \langle p_k\rangle^{n}_{*}\right], \tag{33}$$

where the pressure at level k averaged over the departure area is given by

$$\langle p_k\rangle^{n}_{*} = \frac{1}{\delta A^n_k}\iint_{\delta A^n_k} S(\langle p_k\rangle)\, dA, \tag{34}$$

(Figure 1). Also here the values obtained in the last iteration are used. The explicit CISL thermodynamic equation then becomes

$$\langle T_k\rangle^{n+1}_{\text{expl}} = (T^n_k)_* + \Delta t\, R_d \left[\left(\frac{T_v}{c_p}\right)^n_* + \left(\frac{\widetilde{T}^{n+1}_v}{\widetilde{c}^{\,n+1}_p}\right)\right] \times \left[\frac{\langle p_k\rangle^{n+1}_{\text{expl}} - \langle p_k\rangle^{n}_{*}}{\langle p\rangle^{n+1}_{\text{expl}} + \langle p_k\rangle^{n}_{*}}\right]. \tag{35}$$

3.4 The semi-implicit CISL equations

In this Section the derivation of a semi-implicit system of prognostic equations from the system of explicit equations is described briefly. The derivation is described in more details in Lauritzen (2005) and Machenhauer *et al.* (2007). All steps in a complete derivation will not be dealt with here. We will focus on steps that deviate from the traditional semi-implicit system of HIRLAM that is derived in Undén (2002). Central parts of the derivation are similar to those described for the CISL shallow water model of Lauritzen *et al.* (2006).

Let us summarize the steps involved in a complete derivation. First the explicit system is made semi-implicit by averaging in time between time-level n and $(n+1)$:

1. the linearized part of the pressure gradient force in the momentum equations,
2. the linearized divergence term in the continuity equation and
3. the linearized divergence term in the energy conversion term in the thermodynamic equation.

This is done for the present HIRLAM version in Section 3.4.1, 3.4.2, and 3.4.3, respectively. Secondly the formula for the updated surface pressure and temperature (at time level $(n+1)$) are inserted into the formula for the linearized pressure gradient force in the momentum equations. Finally the divergence operator, $\nabla\cdot(\,)$, is applied

DOI: 10.1002/qj

to the momentum equations resulting in the set of coupled elliptic equations with updated divergence as the unknown variable. These insertions and the final derivation of the elliptic system are not repeated here. They are derived similarly and result in a similar elliptic system, a set of coupled Helmholtz equations, as in HIRLAM. The reader is referred to Undén (2002) or Lauritzen (2005) for details. The final solution to the elliptic system determines the semi-implicit corrections to the explicit solutions for all the prognostic variables.

3.4.1 *The linearized pressure gradient force*

The pressure gradient force at level k

$$PGF_k = -\frac{R_d(T_v)_k}{p_k}\nabla p_k - \nabla\Phi_k = -\frac{R_d\,(T_v)_k}{p_k}\nabla p_k - \nabla\left\{\Phi_s + R_d\sum_{l=k+1}^{NLEV}(T_v)_l\,(\Delta\ln p)_l + \alpha_k R_d(T_v)_k\right\}, \tag{36}$$

is linearized and temporary averaged as in HIRLAM. The result is

$$-\nabla G_k = -\nabla\Bigg[\Phi_s + \frac{R_d}{2}\sum_{l=k+1}^{NLEV}\left\{(T_v)_l^n + \left(\widetilde{T}_v\right)_l^{n+1}\right\}(\Delta\ln p^{\rm ref})_l + \frac{R_d\alpha_k^{\rm ref}}{2}\left\{(T_v)_l^n + \left(\widetilde{T}_v\right)_l^{n+1}\right\}\Bigg] - \frac{R_d T^{\rm ref}}{2p_s^{\rm ref}}\nabla\left(\langle p_s\rangle^n + \langle\widetilde{p}_s\rangle^{n+1}\right), \tag{37}$$

where $T^{\rm ref}$ and $p_s^{\rm ref}$ is a constant reference temperature and a constant reference surface pressure, respectively. $(\Delta\ln p^{\rm ref})_k$ and $\alpha_s^{\rm ref}$ are defined by (16) and (20) with the half level pressures obtained from (13) by choosing $p_s = p_s^{\rm ref}$. See also Appendix A for a suggestion for an alternative Lagrangian discretization of the pressure gradient force.

3.4.2 *The semi-implicit CISL continuity equation*

The discretization of the explicit continuity equation was discussed in Section 3.3. The derivation of the semi-implicit continuity equation considered here is a direct extension of the derivation for the shallow water model in Lauritzen *et al.* (2006). Defining the discretized Lagrangian divergence

$$\mathbb{D}_k^{n+1/2} = \frac{1}{\Delta A}\frac{\Delta A - \delta A_k^n}{\Delta t} = \frac{1}{\Delta t}\left(1 - \frac{\delta A_k^n}{\Delta A}\right), \tag{38}$$

and substituting $\delta A_k^n/\Delta A$ from the explicit continuity equation (24) in the form

$$\langle\delta p_k\rangle_{\rm expl}^{n+1} = \langle\Delta p_k\rangle_*^n\frac{(\delta A_k^n)}{\Delta A}, \tag{39}$$

it may be written as

$$\langle p_k\rangle_{\rm expl}^{n+1} = \langle\Delta p_k\rangle_*^n - \Delta t\langle\Delta p_k\rangle_*^n\mathbb{D}_k^{n+1/2} \tag{40}$$

$$= \langle\Delta p_k\rangle_*^n - \Delta t\left\{\langle\Delta p_k\rangle_*^n\right\}'\mathbb{D}_k^{n+1/2} - \Delta t\,(\Delta p_k)^{\rm ref}\,\mathbb{D}_k^{n+1/2}, \tag{41}$$

where the superscript ‘’’ refers to the deviation from the reference value. Treating the linear term as a temporal average the (‘ideal’) semi-implicit continuity equation yields

$$\langle\delta p_k\rangle^{n+1} = \langle\delta p_k\rangle_{\rm expl}^{n+1} - \frac{\Delta t}{2}(\Delta p_k)^{\rm ref}\left\{\widetilde{\mathbb{D}}_k^{n+1} + \mathbb{D}_k^n - 2\left(\mathbb{D}_k^{n+1/2}\right)\right\}, \tag{42}$$

or

$$\langle\delta p_k\rangle^{n+1} = \langle\delta p_k\rangle_{\rm expl}^{n+1} - \frac{\Delta t}{2}(\Delta p_k)^{\rm ref}\left\{\mathbb{D}_k^{n+1} - \widetilde{\mathbb{D}}_k^{n+1}\right\}, \tag{43}$$

where $\widetilde{\mathbb{D}}_k^{n+1}$ is defined as the Lagrangian divergence for the last part of the hybrid trajectory

$$\widetilde{\mathbb{D}}_k^{n+1} = \widetilde{\mathbb{D}}_k^{n+1}\left(\widetilde{\mathbf{V}}_k^{n+1}\right) = \frac{1}{\Delta A}\frac{\Delta A - \delta A_k^{n+1/2}}{\Delta t}, \tag{44}$$

and

$$\mathbb{D}_k^n = \mathbb{D}_k^n\left(\mathbf{V}_k^n\right) = \frac{1}{\Delta A}\frac{\delta A_k^{n+1/2} - \delta A_k^n}{\Delta t}. \tag{45}$$

Thus,

$$\mathbb{D}_k^n + \mathbb{D}_k^{n+1} = 2\mathbb{D}_k^{n+1/2}. \tag{46}$$

This was used to derive (43) from (42).

In order to proceed with the derivation of the semi-implicit system the predictor-corrector approach from Lauritzen *et al.* (2006) is introduced. This results in elliptic equations in the same simple form as in HIRLAM. The predictor-corrector approach is given by

$$\langle\delta p_k\rangle^{n+1} = \langle\delta p_k\rangle_{\rm expl}^{n+1} - \frac{\Delta t}{2}(\Delta p_k)^{\rm ref}\left(D_k^{n+1} - \widetilde{\mathbb{D}}_k^{n+1}\right) + \frac{\Delta t}{2}(\Delta p_k)^{\rm ref}\langle D_k - \mathbb{D}_k\rangle_*^n\frac{\delta A_k^n}{\Delta A}, \tag{47}$$

where the discretized Eulerian divergence D_k^n is defined in the C-grid in spherical coordinates as

$$D_k^n = \frac{1}{a\cos\theta}\left\{\frac{\delta_\lambda u_k^n}{\Delta\lambda} + \frac{\delta_\theta\,(v_k^n\cos\theta)}{\Delta\theta}\right\} \tag{48}$$

$$= \frac{\delta_\lambda u_k^n}{\Delta x} + \frac{1}{\cos\theta}\frac{\delta_\theta\,(v_k^n\cos\theta)}{\Delta y}, \tag{49}$$

where $\Delta x = a\cos\theta\Delta\lambda$, $\Delta y = a\Delta\theta$, and $\delta_\lambda()$ is a centered finite difference over a grid distance in longitude. $\delta_\theta()$ is defined similarly. The updated surface pressure is the

DOI: 10.1002/qj

weight of the air in the arrival column, so it is obtained by summing (47) over all NLEV layers.

As shown in Section 3.3 the explicit continuity equation is conserving mass exactly, both locally and globally. Since the correction terms in (47), which correct the explicit prediction, consist of linear divergence terms, integration of these terms over the entire integration area is zero if the Lagrangian and the Eulerian divergence is zero at the boundaries or if the integration area is global. Consequently, with these assumptions fulfilled, the semi-implicit continuity equation also conserves global mass. It is the author's impression from preliminary tests that the semi-implicit correction terms generally are small compared to the explicit local mass changes, so it is our impression that the local mass-conservation is only slightly modified by the semi-implicit corrections.

3.4.3 *The semi-implicit version of the thermodynamic equation*

Also a linear dependence on divergence in the thermodynamic equation (4) needs to be temporary averaged in the semi-implicit model version. Specifically, it is the energy conversion term $(R_d T_v\,\omega)/(c_p p)$, approximated in the explicit model with (35), that is divergence dependent. To isolate this dependence $\langle\omega_k\rangle^{n+1/2}$, given by (33), is expanded as follows

$$\langle\omega_k\rangle^{n+1/2}_{\text{expl}} = \frac{1}{\Delta t}\left(\langle p_k\rangle^{n+1}_{\text{expl}} - \langle p_k\rangle^{n}_{*}\right) \tag{50}$$

$$= \frac{1}{\Delta t}\left\{\exp\langle\alpha_k\rangle^{n+1}\sum_{l=1}^{k}\langle p_l\rangle^{n+1}_{\text{expl}} - \langle p_k\rangle^{n}_{*}\right\}, \tag{51}$$

where (21) and (29) have been used. When $\langle p_k\rangle^{n+1}_{\text{expl}}$ is substituted from (39) the result is

$$\langle\omega_k\rangle^{n+1/2}_{\text{expl}} = \frac{1}{\Delta t}\left\{\exp\langle\alpha_k\rangle^{n+1}\sum_{l=1}^{k}\langle\Delta p_k\rangle^{n}_{*} - \langle p_k\rangle^{n}_{*}\right\}$$
$$- \exp\langle\alpha_k\rangle^{n+1}\sum_{l=1}^{k}\langle\Delta p_k\rangle^{n}_{*}\mathbb{D}_l^{n+1/2}. \tag{52}$$

When (52) is inserted in the explicit thermodynamic equation, the result is linearized about a reference temperature T^{ref} and surface pressure p_s^{ref}, and the linear term is temporary averaged, we get the ('ideal') semi-implicit thermodynamic equation

$$T_k^{n+1} = (T_k)^{n+1}_{\text{expl}} - \frac{\Delta t R_d}{c_{pd}}\left(\frac{T}{p_{k+1/2}}\right)^{\text{ref}}\times$$
$$\sum_{l=1}^{k}(\Delta p_l)^{\text{ref}}\left\{\mathbb{D}_l^{n+1} - \widetilde{\mathbb{D}}_l^{n+1}\right\}, \tag{53}$$

where again $\widetilde{\mathbb{D}}_l^{n+1}$ is defined by (44). In order to obtain the same uncomplicated elliptic equations as in HIRLAM the predictor-corrector approach of Lauritzen *et al.* (2006) is again utilized. This changes (53) to

$$T_k^{n+1} = (T_k)^{n+1}_{\text{expl}} - \frac{\Delta t R_d}{c_{pd}}\left(\frac{T}{p_{k+1/2}}\right)^{\text{ref}}\times$$
$$\sum_{l=1}^{k}(\Delta p_l)^{\text{ref}}\left[\left\{D_l^{n+1} - \widetilde{\mathbb{D}}_l^{n+1}\right\}\right.$$
$$\left. - \langle D_l - \mathbb{D}_l\rangle^{n}_{*}\frac{\delta A_l^n}{\Delta A}\right]. \tag{54}$$

3.5 Continuity equations for tracers

The explicit continuity equations for humidity, cloud water, and other atmospheric constituents or tracers are similar to the one for moist air, equation (24), except that they are derived using the densities of the constituents in question $\rho_i = Q_i\rho$ instead of the density of moist air. Here Q_i is the *specific concentration* of the constituent. It is defined as the ratio between the mass of the constituent and the mass of the *moist air* it is mixed into.

The tracer mass in a Lagrangian cell with thickness $\delta z = z_2 - z_1$ is at a certain time:

$$M_{q_i,\delta V} = \iint_{\delta A}\left(\int_{z_1}^{z_2} Q_i\rho\,dz\right)dA \tag{55}$$

$$= \frac{1}{g}\iint_{\delta A} q_i\,\delta p\,dA \tag{56}$$

$$= \frac{1}{g}\langle q_i\delta p\rangle\delta A, \tag{57}$$

where the hydrostatic equation $dp = -g\rho\,dz$ was used in the inner integral and a vertical averaged value, defined by $q_i\delta p = -g\int_{p_1}^{p_2} Q_i\,dp$, was introduced. Thus, the condition for *local tracer mass-conservation* is

$$\frac{dM_{\delta V}}{dt} = \frac{1}{g}\frac{d}{dt}\left(\langle q_i\delta p\rangle\delta A\right) = 0. \tag{58}$$

This is valid only for passive tracers. For non-passive tracers, as water vapor and cloud water, source and sink terms must be added on the right-hand side of (58). The *explicit CISL continuity equation for a passive tracer* is obtained from (58) by integration in time from $n\Delta t$ to $(n+1)\Delta t$. The result is

$$\langle(q_i)_k\,\delta p_k\rangle^{n+1}_{\text{expl}} = \langle(q_i)_k\,\Delta p_k\rangle^{n}_{*}\frac{\delta A_k^n}{\Delta A}. \tag{59}$$

The trajectories determined for the moist air continuity equation is used for the tracers as well, so the upstream integrations in (59) are performed over the same upstream areas δA_k^n as those in (24).

The conservation properties for explicit unforced predictions (59) for limited area models, as the new HIRLAM version, are as described in Section 3.3 for moist air. That is, (59) ensure *global tracer mass-conservation*. This is proven as for moist air (see Section 3.3).

So far only preliminary test runs with humidity and cloud water variables included have been made. No other

DOI: 10.1002/qj

tracer variables were included. In these preliminary tests of the new HIRLAM version the explicit form of the tracer continuity equations (59), with appropriate forcing terms, were used. This form is not completely consistent with the semi-implicit continuity equation (47) used for the moist air, as (59) does not degenerate to (47) if the initial and the reference specific concentrations Q_i are set to 1. Theoretically one can obtain such a consistency by making similar corrections to the explicit tracer predictions as were made to the explicit moist air predictions, i.e. instead of using (59) the following 'semi-implicit' tracer continuity equation

$$\begin{aligned}\langle (q_i)_k\, \delta p_k\rangle^{n+1} &= \langle (q_i)_k\, \delta p_k\rangle^{n+1}_{\text{expl}} \\ &- \frac{\Delta t}{2}\left[(q_i)_k\, \Delta p_k\right]^{\text{ref}} \left(D - \widetilde{\mathbb{D}}\right)_k^{n+1} \\ &+ \frac{\Delta t}{2}\left[(q_i)_k\, \Delta p_k\right]^{\text{ref}} \langle D_k - \mathbb{D}_k\rangle_*^n \frac{\delta A_k^n}{\Delta A}. \quad (60)\end{aligned}$$

It is seen that the right-hand side with $(q_i)_k^0 \equiv 1$ and $(q_i)_k^{\text{ref}} \equiv 1$ degenerates to the right-hand side of (47). If (60) is practical will depend, especially, on the magnitude of the difference between explicit predictions with (59) and 'semi-implicit' predictions with (60). In this paper we use the explicit tracer transport equation (59).

3.6 Vertical remapping and interpolation

Each of the preliminary updated tracer densities $\langle (q_i)_k\, \delta p_k\rangle^{n+1}$, obtained from (60) (or from (59)) at the end of a time step, is an average over a Lagrangian layer $\langle \delta p_k\rangle^{n+1}$. The preliminary values must be remapped to become averaged values over the updated Eulerian model layers $\langle \Delta p_k^{eul}\rangle^{n+1} = \langle p_{k+1/2}^{eul}\rangle^{n+1} - \langle p_{k-1/2}^{eul}\rangle^{n+1}$. This vertical remapping is based on a piecewise parabolic sub-grid scale representation (Colella and Woodward 1984), except at the top and at the surface where piecewise constant representations are applied. Higher-order reconstructions based on extrapolations near the boundaries could be expected to improve accuracy but this was not explored in this preliminary study.

Likewise the updated grid point values T_k^{n+1}, u_k^{n+1} and v_k^{n+1} are given at the end of each time step at the updated discrete Lagrangian levels $\langle p_k\rangle^{n+1} = \exp\langle \alpha_k\rangle^{n+1} \langle p_{k+1/2}\rangle^{n+1}$. They must be interpolated to the discrete Eulerian model levels $\langle p_k^{eul}\rangle^{n+1} = \exp\langle \alpha_k^{eul}\rangle^{n+1} \langle p_{k+1/2}^{eul}\rangle^{n+1}$. Since the prognostic equations for the velocity components and temperature are solved with a grid-point semi-Lagrangian scheme based on cubic Lagrange interpolation, we also use cubic Lagrange interpolation for the vertical remapping of these variables.

In the present approach at the end of each time step the vertical mean values of tracer densities over Lagrangian layers are remapped to become averaged values over the Eulerian model layers. This gives rise to a certain smoothing or damping of the density fields. To minimize this damping it may be considered to keep the Lagrangian layer mean values for a number of consecutive time steps before performing the actual remapping to Eulerian model layer mean values. This could be done simply by letting the arrival cells of the previous time step be the departure cells of the new time step. In the finite volume integrations of Lin (2004) the final vertical remapping of the dynamical prognostic variables were postponed successfully for several consecutive short explicit time steps. So, it seems likely that the Lagrangian layer mean values and the Lagrangian level values may be kept without remapping and interpolation even for several large semi-implicit time steps. Present parameterization schemes need Eulerian model layer mean values or Eulerian model level values. So, at time steps between final remappings and interpolations special remappings and interpolation may be performed for the purpose of parameterization.

As an alternative to the vertical remapping and interpolation procedure chosen here the mass, momentum and total energy conserving vertical remapping algorithm presented in Lin (2004) might be applied. To do that the updated gridpoint values of temperature and velocity components obtained here at the Lagrangian levels at the end of a time step must be interpreted as averaged values over the corresponding Lagrangian levels. The computationally more expensive Lin(2004) algorithm might prove to be more accurate than the present procedure because total energy in a closed system is conserved in the Lin (2004) algorithm and dissipated kinetic energy is consistently converted locally to total potential energy, an effect which is not explicitly included in HIRLAM. A problem seems, however, to be that the energy-conserving vertical remapping introduces spurious contributions to the pressure gradient force leading to unphysical temperature profiles at the model top (C.-C. Chen personal communication).

4 Preliminary test results

The Jablonowski-Williamson baroclinic wave test case consists of an analytic steady-state zonal solution to the global primitive equations (Jablonowski and Williamson 2006; hereafter referred to as JW06). The steady-state surface pressure is constant 1000 hPa. The steady-state is unstable so that an overlaid perturbation triggers the development of an idealized baroclinic wave in the Northern Hemisphere. By day 4 a well-defined wave train is established, and by day 7-9 a significant deepening of the highs and lows takes place before a break down by day 20-30 leads to a full circulation in both hemispheres.

The limited integration area of HIRLAM, in which the new model version has been implemented, is not prepared for an extension to a global domain. In the meridional direction both poles cannot be included in the integration area and in the zonal direction periodic boundaries cannot be used due to the elliptic solver in HIRLAM. Due to these technical issues it would be difficult to extend the integration area of HIRLAM to a

DOI: 10.1002/qj

complete global domain. We choose to make the limited-area domain as global as possible and try to minimize the effects of the boundaries. The active domain extends meridionally from $80°$S to $80°$N, and zonally $360°$ from $80°$W to $280°$E. The zonal extension is chosen such that the initial perturbation, centred at ($20°$E,$40°$N), is far away from the western domain boundary (exactly $100°$). The relaxation zone is located just inside the boundary of the active domain. Within this zone the updated values are relaxed toward the initial values with a weight that decreases from 1 at the boundary to zero at approximately $6°$ from it. To accommodate the CISL schemes there is a halo zone around the active domain in which the fields are held fixed at their initial value.

Two horizontal resolutions are used. The lower resolution is $\Delta\lambda \approx 1.45°$, $\Delta\theta \approx 1.15°$, and the highest resolution is $\Delta\lambda \approx 0.74°$, $\Delta\theta \approx 0.59°$. In the vertical there are 27 levels and the placement of the levels is as in JW06, but with one more layer added at the top of the atmosphere (so that the pressure at the upper boundary is zero as in HIRLAM). The time-step for the low- and high-resolution runs is 30 and 15 minutes, respectively.

The new dynamical cores do not use decentering or filtering of the non-linear terms in time as in HIRLAM, but it was necessary to retain horizontal diffusion in order to avoid noise problems. All integrations were run with ∇^6 implicit horizontal diffusion on T, u and v (see p.12-13 in Undén 2002). The horizontal diffusion coefficients are based on HIRLAM default values scaled for resolution so that the e-folding time of the $2\Delta x$ wave is the same regardless of resolution (McDonald 1998). There has been no attempt to tune the diffusion coefficients for these idealized runs.

In the shallow-water model of LKM06 the constant horizontal mean geopotential used for the semi-implicit scheme was chosen sufficiently large to avoid instabilities because of the 'predictor-corrector' approach applied in the semi-implicit CISL scheme. In a baroclinic model that corresponds to an increase in the reference temperature so that the equivalent depths are increased. In HIRLAM the reference temperature is set to 300 K and in the new dynamical core version it is set to 360 K. The reference surface pressure is unchanged 1000 hPa.

The boundaries introduce effects that are not present in the global model runs. The boundary relaxation and the elliptic solver trigger a weak wave, hereinafter referred to as the *boundary wave* (Fig. 2b), with a structure that is very similar to the large amplitude wave train, hereinafter referred to as the *main wave*, triggered by the overlaid velocity perturbation (Fig. 2a). The *boundary wave* is approximately symmetric about the equator and located in the mid-latitudes. By comparing runs with and without the initial overlaid perturbation on the balanced initial state, it is seen that the *boundary wave* is very similar in the two runs and, thus, the *boundary wave* is not a result of boundary reflections of fast waves triggered by the overlaid velocity perturbation (not shown). The *boundary wave* grows as it propagates eastward just as the main wave train does, and with variation on the order of 1-2 hPa around day 7 after which the deepening accelerates. By placing the velocity perturbation $100°$ from the western boundary, where the *boundary wave* is triggered, the *main wave* and *boundary wave* are initially located far from each other and, hence, the interaction between the two waves is minimized. In the following analysis it is assumed that the *boundary wave* does not interact non-linearly with the *main wave* train, and that the gravity waves triggered by the perturbation do not interact with the *boundary wave*. Under this assumption the *boundary wave* can be 'removed' from the flow by subtracting the deviation from 1000 hPa in the unperturbed run from the perturbed run. As showed on Fig. 2c this is a reasonable operation, that makes the comparison of the limited-area model runs with global model reference solutions feasible.

The error measures defined in JW06 are used to assess the accuracy and convergence characteristics of the new CISL HIRLAM version. Since an analytical solution is not available, JW06 provided high-resolution reference solutions computed with four different dynamical cores. These provide independent estimates of the true solution. JW06 defined the uncertainty for any reference solutions as the maximum deviation in terms of the l_2 error measure between the highest and second highest horizontal resolution runs of all model versions (see JW06 for details). The uncertainty is marked with the shaded region on Fig. 3, hence, a model integration has converged when its l_2 difference is located in the shaded area. For the computation of the l_2 differences the reference solution from the finite-volume dynamical core of the NCAR Community Atmosphere Model (CAM) version 3 is used (Lin 2004). The resolution of the CAM reference solution is $(\Delta\lambda, \Delta\theta) = (0.3125°, 0.25°)$.

Fig. 3 shows the l_2 differences for different HIRLAM versions. First of all it can be seen that up to day 8 both the HIRLAM (reference) and the CISL-HIRLAM have converged in the high-resolution runs (Fig. 3a). After day eight the wave is too close to the boundaries and cannot be compared with the global model simulations provided by JW06. Before approximately day 5 the wave train has very little amplitude and l_2 differences reflect interpolation errors rather than forecast skill. For the lower resolution runs the CISL version of HIRLAM has not converged whereas HIRLAM has, so the finite-volume model needs higher resolution than the grid-point model to get the same level of accuracy. This has also been observed for the finite-volume dynamical core in CAM (Lin 2004), which needs higher resolution to reach the same level of accuracy as the lower-resolution spectral dynamical core of CAM (JW06). Regarding phase errors (not shown) the CISL-HIRLAM performs slightly better than HIRLAM at both resolutions. When using the cascade scheme of Nair *et al.* (2002) instead of the fully two-dimensional CISL scheme of Nair and Machenhauer (2002) the accuracy in terms of the l_2 difference is not altered (Fig. 3b). The importance of the consistent Lagrangian discretization of the energy conversion term introduced in Section 3 is demonstrated on Fig. 3c. The l_2 differences and phase errors (not shown) are larger when using the Eulerian

DOI: 10.1002/qj

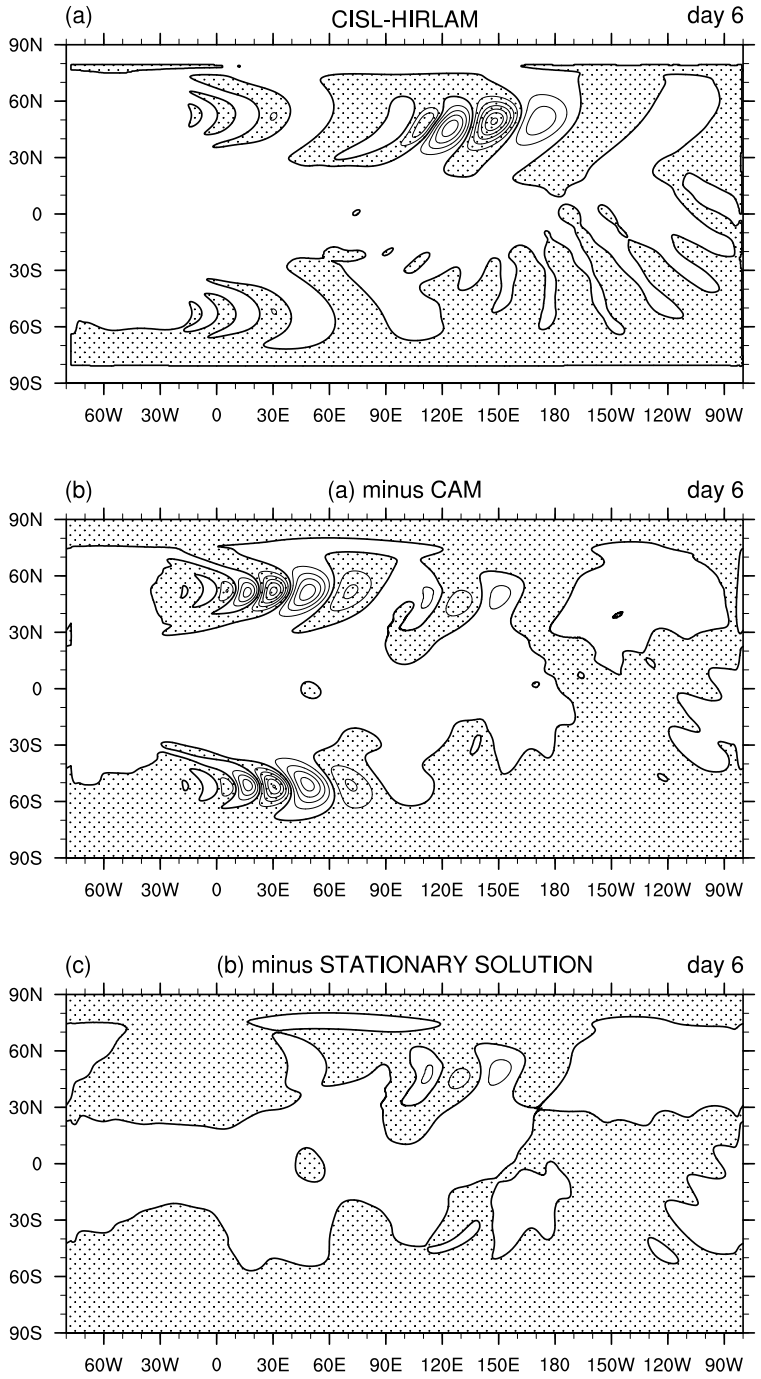

Figure 2. (a) shows the surface pressure, p_s, in hPa at day 6 for the Jablonowski-Williamson baroclinic wave test case for the high-resolution run with CISL-HIRLAM. Thick solid contour is 1000 hPa, the contour interval is 1 hPa and shaded region marks values below 1000 hPa. The *main wave* is located from approximately $90E$ to $160W$ in the northern hemisphere. (b) When subtracting the CAM reference solution from the CISL-HIRLAM data the *boundary wave*, which is triggered by the boundary relaxation and elliptic solver in HIRLAM, becomes clearly visible. The thick solid contour is 0 hPa, the contour interval is 0.2 hPa and shaded region marks negative values. The boundary wave is also present in the unperturbed CISL-HIRLAM run that does not contain the *main wave*. (c) shows the CAM reference solution and the unperturbed CISL-HIRLAM solution subtracted from the perturbed CISL-HIRLAM solution. This demonstrates that the *boundary wave* can, to a first approximation, be 'removed'. Contours in (c) are the same as in (b).

treatment of the conversion term (R-CISL) compared to the Lagrangian discretization presented herein.

CISL-HIRLAM has also been coupled with the HIRLAM physics package and initial tests run from the initial condition of a strongly developing extra-tropical storm have been performed (not shown). The new model version ran stably and produced simulations quite similar to REF-HIRLAM. Also for the full-physics run the Lagrangian discretization of the energy-conversion term lead to more accurate simulations compared to the traditional discretization.

DOI: 10.1002/qj

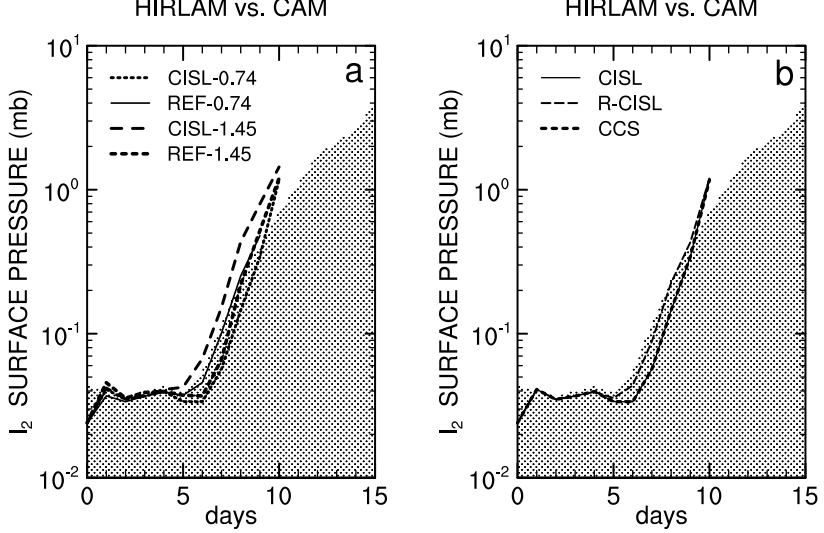

Figure 3. The Figure shows l_2 norms of the surface pressure differences (in hPa) between HIRLAM versions and the CAM global reference solution as a function of time. The shaded region is the uncertainty of the reference solutions defined in JW06. (a) show l_2 differences for the high(short dashed line)/low(long dashed line) resolution CISL-HIRLAM and the high(solid line)/low(dashed line) resolution standard HIRLAM (REF). (b) show l_2 differences for high-resolution versions of CISL-HIRLAM: solid line is CISL-HIRLAM based on the two-dimensional CISL scheme of Nair and Machenhauer (2002), dashed lines is CISL-HIRLAM based on the conservative cascade scheme (CCS) of Nair *et al.* (2002), and long dashed lines is CISL-HIRLAM using the traditional Eulerian discretization of the energy-conversion term in the thermodynamic equation (R-CISL). Note that the choice of advection scheme does not alter the accuracy of the solution in terms of l_2 and that the traditional treatment of the energy conversion term in the thermodynamic equation leads to less accurate solutions compared to the Lagrangian discretization presented in this paper.

5 Conclusions and discussion

It has been demonstrated that the semi-implicit semi-Lagrangian primitive equation model HIRLAM can be rendered mass-conservative by combining a cell-integrated semi-Lagrangian (CISL) version of the continuity equation with the grid point form of the prognostic momentum and thermodynamic equations. Long time steps are obtained with the application of the recently developed predictor-corrector method of Lauritzen *et al.* (2006) that results in the same non-complicated elliptic equations as in the semi-implicit scheme of HIRLAM. Contrarily to traditional approaches in semi-Lagrangian models, the vertical displacements of Lagrangian mass cells in the new model version are determined without use of time extrapolated vertical velocities. They are diagnosed from their horizontal displacements, determined from the horizontal flow and maintenance of hydrostatic balance. This is used to diagnose vertical velocities that discretize the energy conversion term in the thermodynamic equation in a Lagrangian fashion.

The new dynamical core has been validated using a recently developed idealized baroclinic wave test case for global dynamical cores (Jablonowski and Williamson 2006). Except for a slight smoothing of a low resolution run the new model version was found to be accurate compared to a high-resolution global reference simulation when the artifacts introduced at the limited-area boundaries were, at least to first order, removed from the flow. The model has also been coupled to HIRLAM physics, and stable 48-hour forecasts from an initial condition leading to a strong extra-tropical cyclone development have been performed but not reported on here. A main finding in both test cases is that the new model version based on the Lagrangian discretization of the energy conversion term in the thermodynamic equation was significantly more accurate than when using the traditional Eulerian treatment of the conversion term.

The model version presented here is for a limited area on the sphere. For wider applications, an extension to a full global domain is, of course, needed. No serious problems is expected in such an extension, especially as both advection schemes used here have originally been formulated on the sphere, both using the same local approach for accurate transport over the polar regions. Also, the discretization of the pressure gradient force may be performed in a Lagrangian fashion as outlined in Appendix A. As described in Machenhauer *et al.* (2007), we note that the approach of solving the CISL continuity equation via a two dimensional upstream integration is not only valid in the quasi-hydrostatic case. This method is general and can be used to extend the CISL-HIRLAM scheme to the non-hydrostatic case.

Acknowledgements

This work was supported by the Copenhagen Global Change Initiative, the Danish Meteorological Institute, and the Advanced Study Program at the National Center for Atmospheric Research, and by the Centre for Energy Environment and Health (www.ceeh.dk). The first author is grateful to David L. Williamson for computing error measures and associated figures. Ramachandran D. Nair and David L. Williamson are acknowledged for helping

DOI: 10.1002/qj

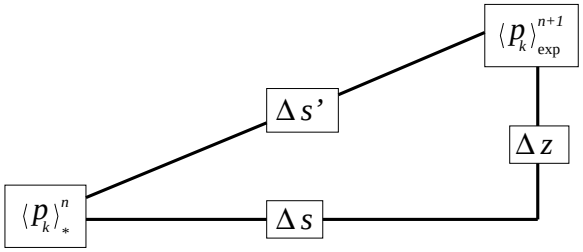

Figure 4. A graphical illustration of the computation of the pressure gradient force (see text for details).

clarifying the initial versions of this manuscript, and also two anonymous reviewers for their helpful comments.

Appendix A: Suggestion for a Lagrangian pressure gradient force discretization

Lin (1997) derived an Eulerian expression for the horizontal pressure gradient force aiming at an elimination of the well-known inaccuracy caused by different truncation errors in the two terms that the pressure gradient force traditionally is split into when using terrain following coordinates (see (1) and (2)). As illustrated in Figure 4 the pressures $\langle p_k \rangle^{n+1}_{\text{expl}}$ and $\langle p_k \rangle^{n}_{*}$ can be used to determine a similar Lagrangian mean value of the explicit horizontal pressure gradient force (PGF_h) acting upon a Lagrangian mass cell moving with the three dimensional flow along a hybrid trajectory. The mean pressure gradient force along the sloping hybrid trajectory is

$$PGF_s = \left[\left(-\frac{1}{\rho} \frac{\partial p}{\partial s'} \right)_k \right]^{n+1/2}_{\text{expl}} \tag{61}$$

$$= -\frac{1}{\langle \rho \rangle} \frac{\langle p_k \rangle^{n+1}_{\text{expl}} - \langle p_k \rangle^{n}_{*}}{\Delta s'} \tag{62}$$

$$= -\frac{1}{\langle \rho \rangle} \frac{\langle p_k \rangle^{n+1}_{\text{expl}} - \langle p_k \rangle^{n}_{*}}{\Delta s} \cos(\varphi), \tag{63}$$

where $\langle \rho \rangle$ is an approximation to the mean density along the hybrid trajectory (e.g. the arithmetic mean value of the density of the mass cell at the arrival and the departure positions), Δs is the horizontal distance between the mid points of the mass cells at the arrival and the departure position, and $\Delta s'$ is the corresponding distance along the sloping trajectory (Fig. 4). Thus, φ is the slope of the hybrid trajectory determined by $\tan\varphi = \frac{\Delta z}{\Delta s}$, where Δz is the height difference of the mid points of the mass cells at the arrival and the departure position. In order to determine PGF_h the vertical component of the pressure gradient force, PGF_v, which in a hydrostatic atmosphere is balanced by gravity g, must be subtracted from (61). So,

$$PGF_h = \sqrt{(PGF_s)^2 - g^2}. \tag{64}$$

Instead of approximations of the traditional two-term expressions for the pressure gradient force in the explicit momentum equations (1) and (2), one could consider to use properly interpolated eastward and northward components of PGF_h determined by (61). This must be expected to lead to increased accuracy, even in semi-implicit integrations and even though the linearized pressure gradient force is based on the two-term expression.

References

Colella P, Woodward R. 1984. The piecewise parabolic method (PPM) for gas-dynamical simulations. *J. Comput. Phys.* **54**: 174–201.

Jablonowski C, Williamson D. L. 2006. A baroclinic instability test case for atmospheric model dynamical cores. *Q. J. R. Meteorol. Soc.* **132**: 2943–2975.

Lauritzen P. H. 2005. *An inherently mass-conservative semi-implicit semi-Lagrangian model*. PhD thesis, University of Copenhagen, Denmark.

Lauritzen P. H. 2007. A stability analysis of finite-volume advection schemes permitting long time steps. *Mon. Weather Rev.* **135**: 2658–2673.

Lauritzen P. H., Kaas E., Machenhauer B. 2006. A mass-conservative semi-implicit semi-Lagrangian limited area shallow water model on the sphere. *Mon. Weather Rev.* **134**: 1205–1221.

Lin S. J. 1997. A Finite-Volume Integration Method for Computing the Pressure Forces in General Vertical Coordinates. *Q. J. R. Meteorol. Soc.*, **123**: 1749–1762.

Lin S. J. 2004. A 'vertically Lagrangian' finite-volume dynamical core for global models. *Mon. Weather Rev.* **132**: 2293–2307.

Machenhauer B. 1994. *A mass-, energy- and entrophy conserving semi-Lagrangian and explicit integration scheme for the primitive meteorological equations*. Pp. 73–102 in MPI Tech. Rep. 146, Hamburg, Germany.

Machenhauer B., Kaas E., Lauritzen P. H. 2007. *Finite-volume methods in meteorology*. To appear in *Computational methods for the atmosphere and the oceans*. Ed. R Temam and J Tribbia, ELSEVIER, Amsterdam, The Netherlands.

Machenhauer B., Olk M. 1997. The implementation of the semi-implicit scheme in cell-integrated semi-Lagrangian models. *Atmos.-Ocean* **35**: 103–126.

Machenhauer B., Olk M. 1998. *Design of a semi-implicit cell-integrated semi-Lagrangian model*. Pp. 76–85 in MPI Tech. Rep. 265, Hamburg, Germany.

McDonald A. 1998. *Default horizontal diffusion coefficients in HIRLAM-4.1*. HIRLAM newsletter No.31.

Nair R. D., Machenhauer B. 2002. The mass-conservative cell-integrated semi-Lagrangian advection scheme on the sphere. *Mon. Weather Rev.* **130**: 649–667.

Nair R. D., Scroggs J. S., Semazzi F. H. M. 2002. Efficient conservative global transport schemes for climate and atmospheric chemistry models. *Mon. Weather Rev.* **130**: 2059–2073.

Nair R. D., Tufo H. 2007. Petascale atmospheric general circulation models. *J. Physics: Conference Series.* **78**.

Ritchie H. 1991. Application of the semi-Lagrangian method to a multilevel spectral primitive-equations model. *Q. J. R. Meteorol. Soc.* **117**: 91–106.

Simmons A., Burridge D. 1981. An energy and angular-momentum conserving vertical finite-difference scheme and hybrid vertical coordinates. *Mon. Weather Rev.* **109**: 758–766.

Staniforth A., Côté J. 1991. Semi-Lagrangian integration schemes for atmospheric models - a review. *Mon. Weather Rev.* **119**: 2206–2223.

Starr V. P. 1945. A quasi-Lagrangian system of hydrodynamical equations. *J. Meteor.* **2**: 227–237.

Thuburn J. 2008. A fully implicit, mass-conserving, semi-Lagrangian scheme for the f-plane shallow-water equations. *Int. J. Numer. Meth. Fluids.* **56**: 1047-1059.

Undén P. 2002. *HIRLAM-5 Scientific Documentation*. Pp. 1–144, SMHI, Norrköping, Sweeden.